Results in Engineering 1 (2019) 100001

Contents lists available at ScienceDirect

Results in Engineering

journal homepage: www.editorialmanager.com/rineng/Default.aspx

Analysis of a series hybrid vehicle concept that combines low temperature combustion and biofuels as power source

Antonio García, Javier Monsalve-Serrano *

CMT - Motores Térmicos, Universitat Politècnica de València, Camino de Vera s/n, 46022 Valencia, Spain

ARTICLE INFO

Keywords:
Low temperature combustion
Series hybrid vehicle
Dual-fuel combustion
Alternative fuels
Driving cycles

ABSTRACT

This work evaluates the potential of a series hybrid vehicle concept that combines low temperature combustion (LTC) and biofuels as power source. To do this, experimental data from a previous work obtained in a single-cylinder engine running under ethanol-diesel dual-fuel combustion is used. Then, vehicle systems simulations are used to estimate performance and emissions of the LTC hybrid vehicle and compare them versus conventional diesel combustion (CDC). The vehicle selected to perform the simulations is the Opel Vectra, which equips the compression ignition engine used in the experimental tests.

The results from the simulations used for the analysis are firstly optimized by combining design of experiments and the Kriging fitting method. The multi-objective optimization allows to determine some characteristics and controls of the hybrid vehicle. The comparison of the estimated performance and emissions of the LTC-hybrid concept versus CDC over the worldwide harmonized light vehicles test cycle (WLTC) and real driving cycle (RDE) revealed clear benefits in terms of energy consumption, CO_2 and NOx and soot emissions. In this sense, the hybrid concept enabled a reduction of the final energy consumed of 3% in the RDE cycle and 6.5% in the WLTC as compared to CDC. In terms of engine-out emissions, the CO_2 was reduced around 16% versus CDC, and engine-out NOx and soot were reduced below the levels imposed by the Euro 6 regulation. As a penalty, the engine-out HC and CO emissions increased to more than double than CDC. However, based on previous experimental results, it is expected that a conventional diesel oxidation catalyst can reduce the tail-pipe HC and CO levels below the Euro 6 limits.

Introduction

Over 1.2 billion vehicles are running nowadays in the world, and this number is estimated to increase up to 2 billion by 2035 [1]. Among the different platforms, light-duty vehicles are estimated to make up 95% of that total, with 99% using internal combustion engines (diesel or gasoline fueled) as a power source [2]. In spite of the light-duty vehicles facilitate the daily mobility of the people, the massive use of this technology aggravates the global warming problem and increases the local pollution in the urban areas [3], which has noxious effects to the human health [4]. With this scenario, the necessity of developing alternative vehicle technologies that improve the air quality in the cities is clear. An effective way to reduce the local air pollution is the vehicle electrification. While full electric vehicles are not presumed to have a big share of the vehicle fleet in a short term, hybrid vehicles are expected to have a key role on the close future light-duty vehicle fleet [2].

Hybrid vehicles rely on internal combustion engines (ICE) as power source. Depending on the hybrid vehicle platform, the ICE is used at different degrees. In a series hybrid vehicle (SHV), the primary energy comes from a fossil fuel that is converted into mechanical work through the ICE. Then, the ICE is responsible of driving an electric motor that provides the final power to the vehicle wheels and charges the battery [5]. In a serial-parallel hybrid vehicle, the primary energy also comes from a fossil fuel, but the ICE can be also used to provide direct power to the vehicle wheels [6]. Finally, in the case of the plug-in hybrid electric vehicles (PHEV) part of the primary energy comes from the electrical network, so that the role of the ICE is wanted to be reduced. In any case, since all the hybrid configurations require an ICE, the emissions levels must be controlled to fulfill the targets imposed by the current regulations. To reduce the pollutant levels before being emitted to the atmosphere, the hybrid vehicles need to be equipped with similar aftertreatment systems (ATS) to those used in conventional vehicles (diesel and gasoline) [7]. The addition of the ATS increases the production cost as well as the operation cost of the vehicle because they usage incur in an extra fuel consumption and also needs maintenance [8].

* Corresponding author.
E-mail address: jamonse1@mot.upv.es (J. Monsalve-Serrano).

https://doi.org/10.1016/j.rineng.2019.01.001

Abbreviations

ATS	Aftertreatment Systems
BMEP	Brake Mean Effective Pressure
CAD	Crank Angle Degree
CDC	Conventional Diesel Combustion
CO	Carbon Monoxide
DI	Direct Injection
DOC	Diesel Oxidation Catalysts
DOE	Design of Experiments
DPF	Diesel Particulate Filter
EGR	Exhaust Gas Recirculation
FSN	Filter Smoke Number
HC	Hydro Carbons
HCCI	Homogeneous Charge Compression Ignition
LHV	Lower Heating Value
LTC	Low Temperature Combustion
MON	Motored Octane Number
NOx	Nitrogen Oxides
OEM	Original Equipment Manufacturer
PCI	Premixed Compression Ignition
PFI	Port Fuel Injection
PHEV	Plug-in Hybrid Electric Vehicle
PPC	Partially Premixed Charge
RBC	Rule Based Control
RCCI	Reactivity Controlled Compression Ignition
RDE	Real Driving Emissions
RON	Research Octane Number
SCE	Single Cylinder Engine
SCR	Selective Catalytic Reduction
SHV	Series Hybrid Vehicle
SOC	State of Charge
WLTC	Worldwide harmonized Light vehicles Test Cycle

In parallel to the development of efficient aftertreatment systems, alternative combustion concepts are being investigated nowadays [9]. From the different approaches, the premixed low temperature combustion (LTC) has been proved as the most effective strategy to reduce NOx and soot emissions while maintaining or reducing the fuel consumption [10]. Generally, the LTC takes place in a highly diluted environment with high exhaust gas recirculation (EGR) rates that allows a fast combustion process with reduced heat transfer [11]. Depending on the injection-combustion strategy, different concepts are classified in the literature. The first developed premixed LTC strategy is the homogeneous charge compression ignition (HCCI), which relies on a very early fuel injection timing to obtain a homogeneous mixture of fuel, air and EGR prior the combustion process [12]. This leads to a fast autoignition with a rapid heat release, reducing the time for heat transfer and leading to higher thermal efficiency values than conventional diesel combustion (CDC) [13]. It was also demonstrated that this combination of factors allows to achieve virtually zero NOx and soot emissions [14]. However, a lack of combustion control was observed since the process is entirely dominated by chemical kinetics. After that, the partially premixed combustion (PPC) strategy was proposed aiming to increase the combustion control while maintaining the benefits of HCCI in terms of fuel consumption and emissions. The combustion control improvement was achieved by reducing the homogeneity degree inside the combustion chamber prior to combustion, which was done by delaying the fuel injection timing. However, combustion control at high loads was not possible due to the high reactivity of the diesel fuel [15]. The literature demonstrates that using gasoline fuel extends the ignition delay and allows better control of the PPC at higher loads, but low load operation becomes difficult [16]. Following these conclusions, Inagaki et al. [17] proposed the dual-fuel premixed compression ignition (PCI) concept using separated injection systems to inject two fuels with different reactivity. The authors reported ultra-low NOx and soot emissions and good combustion control using direct injection of diesel and port fuel injection of gasoline. Stable operation at different loads was possible by modifying the fuels proportion depending on the operating conditions. Nowadays, this concept is known as reactivity controlled compression ignition (RCCI). The potential of RCCI has been proved in different engine platforms [18,19] and operating with different fuels [20,21]. All the recent studies confirm the potential of this concept to achieve engine-out NOx and soot levels below the emissions standards with high thermal efficiency [22]. Moreover, an exhaustive characterization about the RCCI emissions composition have been performed [23,24]. The main drawback found with RCCI are the excessive pressure rise rate at high loads if it is wanted to maintain both NOx and soot at ultra-low levels [25]. Moreover, the HC and CO levels at low load are orders of magnitude greater than the regulation limits [26]. Nevertheless, recent studies found that a conventional diesel oxidation catalyst (DOC) used in diesel vehicles could operate with conversion efficiency levels near 97% and 100% for HC and CO, respectively, once the light-off temperature is achieved (~200 °C) [27].

The objective of the current work is to evaluate the potential of coupling two effective technologies for reducing the CO_2 and rest of emissions, the low temperature dual-fuel combustion and the hybrid technology. To do this, a LTC series hybrid vehicle concept is simulated using previous experimental dual-fuel combustion results with ethanol and diesel as fuels. The data analyzed from the simulation is firstly optimized by combining design of experiments and the Kriging fitting method. Then, the results obtained for the hybrid concept are compared to CDC under two different driving cycles, the worldwide harmonized light vehicles test cycle (WLTC) and real driving cycle (RDE). Finally, a DOC model is used to estimate the tail-pipe HC and CO emissions with the hybrid LTC concept.

Materials and methods

Engine, fuels and test cell

The experimental data used in this work were obtained in a single-cylinder diesel engine (SCE) based on a serial production light-duty 1.9 L platform. The engine has four valves driven by dual overhead cams. The piston used is the serial one, with a re-entrant bowl that confers a geometric compression ratio of 17.1:1. The swirl ratio was fixed at 1.4 using the tangential and helical valves located in the intake port [28], which is a representative value of that used in the stock engine configuration. Table 1 summarizes the more relevant characteristics of the engine.

The fuel injection system was adapted to allow RCCI operation as shown in Fig. 1. As sketched, the EN590 diesel fuel was injected into the

Table 1
Engine characteristics.

Engine Type [−]	4 stroke, 4 valves, direct injection
Number of cylinders [−]	1
Displaced volume [cm^3]	477
Stroke [mm]	90.4
Bore [mm]	82
Piston bowl geometry [−]	Re-entrant
Compression ratio [−]	17.1:1
Rated power [kW]	27.5 @ 4000 rpm
Rated torque [Nm]	80 @ 2000–2750 rpm

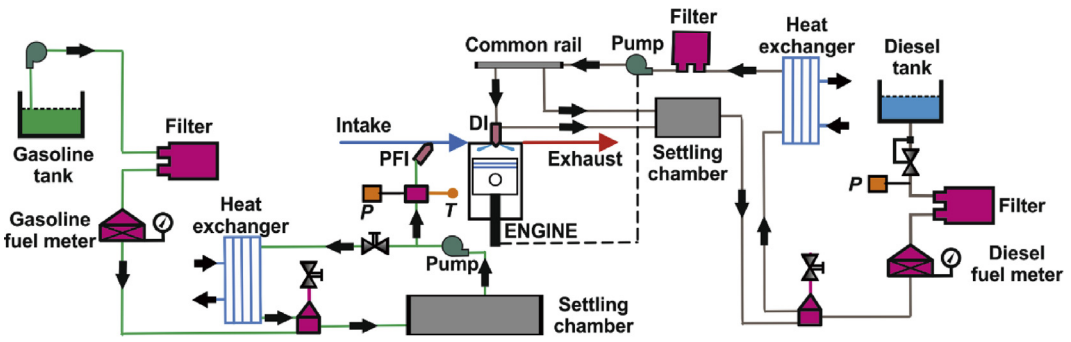

Fig. 1. Fuel injection systems scheme.

cylinder by means of a centrally located solenoid direct injector (DI) coupled with a common-rail fuel injection system. The injection settings were managed using a DRIVVEN controller. The E85 fuel was fumigated in the intake manifold using a port fuel injection (PFI) located 160 mm far from the intake valves, which was governed through a Genotec unit. The mass flow rate of both fuels was measured using dedicated AVL 733S fuel balances. The main characteristics of the DI and PFI are depicted in Table 2, and the most relevant properties of the high and low reactivity fuels used in this study are summarized in Table 3.

The scheme of test cell in which the engine is operated is shown in Fig. 2. An electric dynamometer is used for the engine speed and load control during the experiments. The air intake line is composed of a screw compressor that feeds the engine with fresh air at a pressure up to 3 bar, heat exchanger and air dryer to modify the temperature and relative humidity of the air, airflow meter and a settling chamber sized to attenuate the pulsating flow. Moreover, pressure and temperature transducers are instrumented in this element with regulation purposes. The EGR is introduced in the intake line, downwards the settling chamber, through a dedicated line composed of a heat exchanger, settling chamber and regulation valve. EGR temperature is monitored in several points along the line for its control. Finally, the pressure and temperature of the air-EGR mixture is measured in the intake manifold before entering to the cylinder.

The first elements of the exhaust line are the pressure and temperature transducers located in the exhaust manifold. After them, a settling chamber is installed to attenuate the exhaust flow before the EGR bypass. Later a pneumatic valve is used to reproduce the backpressure provoked by the turbocharger in the real multi-cylinder engine. The last elements of the exhaust line are the emissions analyzers. A five-gas Horiba MEXA-7100 DEGR analyzer is used to measure the gaseous engine-out emissions. Each steady-state operating points is measured three times along a period of 60 s. Finally, an AVL 415S smoke meter is used to measure the smoke emissions in filter smoke number (FSN) units. Three consecutive measurements of 1 L volume each with paper-saving mode off were took at each engine operating point. The accuracy of the main elements of the test cell is shown in Table 4.

Table 2
Characteristics of the direct and port fuel injector.

Direct injector		Port fuel injector	
Actuation Type [−]	Solenoid	Injector Style [−]	Saturated
Steady flow rate @ 100 bar [cm^3/min]	880	Steady flow rate @ 3 bar [cm^3/min]	980
Included spray angle [°]	148	Included Spray Angle [°]	30
Number of holes [−]	7	Injection Strategy [−]	single
Hole diameter [μm]	141	Start of Injection [CAD ATDC]	340
Maximum injection pressure [bar]	1600	Maximum injection pressure [bar]	5.5

Table 3
Physical and chemical properties of the fuels.

	Diesel EN590	E85
Density [kg/m^3] (T = 15 °C)	842	781
Viscosity [mm^2/s] (T = 40 °C)	2.929	–
RON [−]	–	108
MON [−]	–	89
Ethanol content [% vol.]	–	84.7
Cetane number [−]	51	–
Lower heating value [MJ/kg]	42.50	31.56

Vehicle, computational model and driving cycles

The vehicle selected to perform the simulations is the Opel Vectra, which equips the compression ignition engine used in the experimental tests. The aerodynamic and mechanical characteristics of the original equipment manufacturer (OEM) vehicle are described in Table 5. Table 5 also shows the characteristics of the low temperature combustion hybrid vehicle defined for the study, including the additional electrical components.

The vehicle has been modeled in GT- Power® following the data found in the OEM manual. Fig. 3 illustrates the model with the respective sub-assemblies that stand for the different vehicle systems. The model consists of several sub-models as the "VEHICLE" where the majority of the geometric characteristics are defined, "ICE" and the supervisory controller that is responsible to control the SoC and the engine state. Additionally, the electric motors are represented by "GEN" (generator) and "TM" (traction motor). The time speeds profiles are defined in the object "DRIVER", which consists of a PID controller that determine the instantaneous required power to reach the speed demand and actuates on the accelerator position. The engine maps obtained in the bench tests have been used as inputs to the model to allow the determination of the vehicle performance and emissions during each driving cycle. For each instant, the break mean effective pressure (BMEP) values as well as the engine speed are determined. With these two numbers, it is possible to look-up the values of the inserted parameters inside the maps.

Equation (1) relates all the forces that are acting on the vehicle to evaluate the required work to achieve the target speed. It considers parameters as I_{trans1} and I_{trans2} (input and output inertia of the transmission system), I_{dsh} and I_{axl} (driveshaft and axle moment of inertia), R_d and R_t (terms related with the gearbox). ω_{drv} is the instantaneous vehicle speed and is function of the wheel radius (r_{whl}) and vehicle mass M_{veh}, F_{aer}, F_{rol} F_{grd}, are the vehicle mass, aerodynamic forces, rolling resistance forces and gravity forces respectively. For both powertrains the same set of motion equations are solved. Nonetheless, the hybrid system uses additional equations to determine the battery charging, instantaneous state of charge, etc. It is also important to mention than an additional loss term was added to the system for the hybrid powertrain. As the engine remains turned-off long periods of time, every time it is started, an additional fuel consumption will be presented as result of the improved heat losses. Therefore, a fuel penalty was attributed for each engine start and was considered during the simulations.

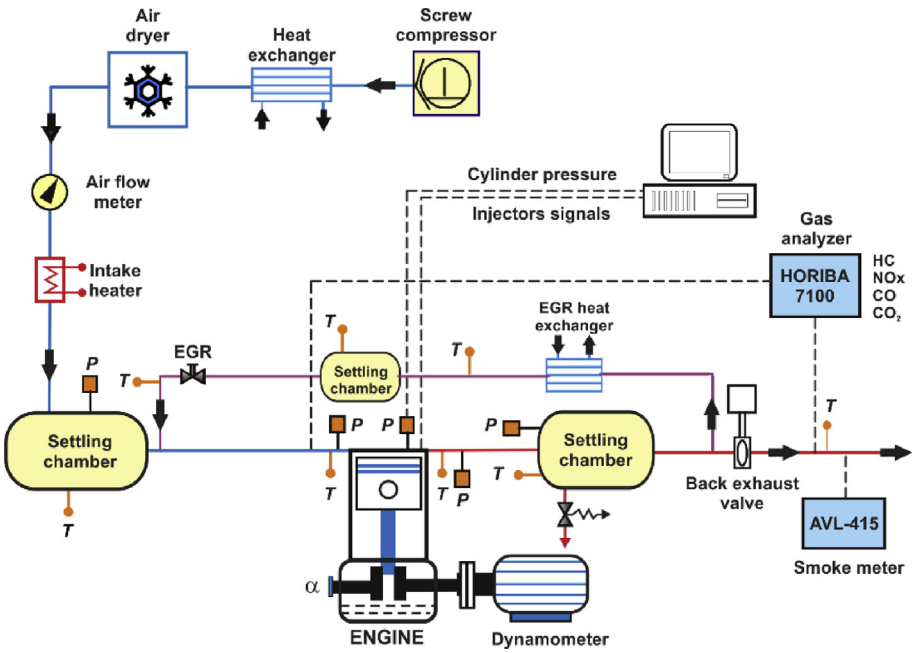

Fig. 2. Test cell scheme.

Table 4
Accuracy of the instrumentation used in this work.

Variable measured	Device	Manufacturer/ model	Accuracy
In-cylinder pressure	Piezoelectric transducer	Kistler/6125BC	±1.25 bar
Intake/exhaust pressure	Piezorresistive transducers	Kistler/4603B10	±25 mbar
Temperature in settling chambers and manifolds	Thermocouple	TC direct/type K	±2.5 °C
Crank angle, engine speed	Encoder	AVL/364	±0.02 CAD
NOx, CO, HC, O_2, CO_2	Gas analyzer	HORIBA/MEXA 7100 DEGR	4%
FSN	Smoke meter	AVL/415	±0.025 FSN
Diesel and E85 fuel mass flow	Fuel balances	AVL/733S	±0.2%
Air mass flow	Air flow meter	Elster/RVG G100	±0.1%

Table 5
Vehicle specifications.

Vehicle type [−]	OEM	LTC-hybrid
Base vehicle Mass [kg]	1573	1573
Passenger and Cargo Mass [kg]	100	100
Vehicle Drag Coefficient [−]	0.28	0.28
Frontal Area [m^2]	2.04	2.04
Tires Size [mm/%/inch]	225/45/ R118	225/45/ R118
Differential ratio [−]	4.1	4.1
Electric motor power [kW]	N/A	105
Generator power [kW]	N/A	55
Weight account by electric motor power [kg/kW]	N/A	0.4
Gear ratio between engine and generator [−]	N/A	2.1
Battery component [−]	N/A	Lithium-Ion
Nominal voltage [V]	N/A	375
Weight account by Battery power [kg/kWh]	N/A	10.5

$$\tau_{vehicle} = \left[I_{trans1} + \frac{I_{trans2}}{R_t^2} + \frac{I_{dsh}}{R_t^2} + \frac{I_{axl}}{(R_d^2)(R_t^2)} + \frac{(M_{veh})(r_{whl}^2)}{(R_d^2)(R_t^2)} \right] \frac{d\omega_{drv}}{dt} - \left[\frac{I_{trans2}}{R_t^3} + \frac{I_{dsh}}{R_t^3} + \frac{I_{axl}}{(R_d^2)(R_t^3)} + \frac{(M_{veh})(r_{whl}^2)}{(R_d^2)(R_t^3)} \right] \omega_{drv} \frac{dR_t}{dt} + \left[\frac{F_{aer} + F_{rol} + F_{grd}}{R_d R_t} \right] r_{whl} \quad (1)$$

The driving cycles selected to be studied in this work are the WLTC and the RDE because they have a major relevance in the current regulatory stages of the European emissions standard. The time-vehicle speed profiles for both cycles are presented in Fig. 4, where the RDE profile come from a previous investigation made by the authors [29]. Comparing both cycles, it is seen that the WLTC cycle has a total duration of 1820 s (≈23 km) whilst the RDE presents a higher duration with a total time of 5580 s (≈67 km). Another difference is the total amount of accelerations and decelerations during the cycle. Since the RDE is based on real urban traffic, there is a higher number of stops and subsequently accelerations than the WLTC, which will have a direct impact on the demanded engine BMEP and engine-out emissions.

Results and discussion

This section is divided into three subsections. The first one shows the performance and emissions maps obtained in the single-cylinder engine, which are used to feed the vehicle model. The second one shows the optimization of the energy management control strategy, which is done by means design of experiments (DoE) coupled with the Kriging fitting method [30]. Finally, the performance and emissions of the LTC-SHV concept with the optimal configuration are evaluated under two driving cycles (WLTC and RDE) and compared to the results obtained with CDC.

Single-cylinder engine maps

The experimental maps obtained from the test bench are presented in Fig. 5. The area falling within the dashed line corresponds to that in which the engine operates under dual-fuel E85-diesel operation. In the rest of the map, the engine runs under conventional diesel combustion.

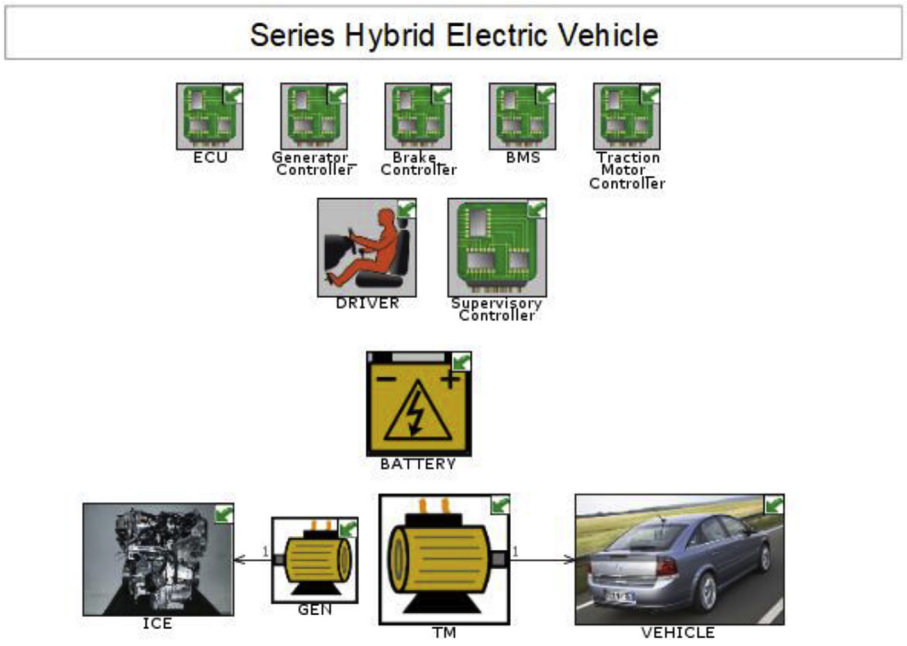

Fig. 3. Vehicle model developed in GT- Power® for the Opel Vectra.

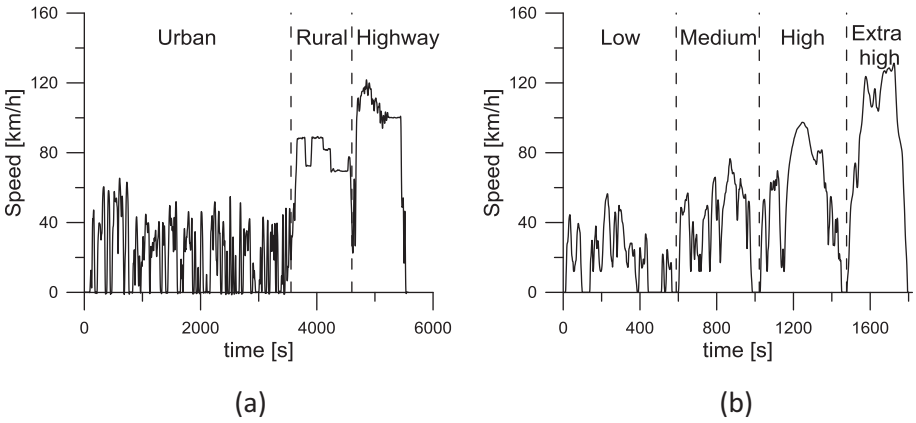

Fig. 4. Time-vehicle speed profiles of the RDE (a) and WLTC (b) cycles [29].

The details of the engine calibration procedure can be found in Ref. [31]. As can be inferred from the maps, the dual-fuel operation allows a notable reduction of NOx, soot and CO_2 emissions as compared to the surrounding diesel operation area. By contrast, CO and HC emissions are notably increased. In terms of BSFC, the figure shows that the dual-fuel portion penalizes the global map. However, part of the BSFC increase is associated to the difference in lower heating value (LHV) between E85 and diesel. So, to perform a fairer comparison, the next analysis will be done in terms of energy consumption instead of grams of fuel. Finally, Fig. 6 shows that the ethanol fraction used in the dual-fuel portion of the map ranges from 40% to 80%.

Optimization of the energy management control strategy

To perform the optimization of the energy management control strategy for the LTC-SHV concept, a methodology combining DoE and the Kriging fitting method is used. It is interesting to note that the optimization is performed for the WLTC cycle, which has a fixed vehicle speed-time profile. After that, the optimal solution will be used to obtain performance and engine-out emissions estimations under both the WLTC and RDE cycle.

In a series hybrid concept, the electric motor is the responsible of moving the vehicle wheels. The thermal engine, in this case running under dual-fuel operation, is only used for sustaining a certain level of battery state of charge (SOC), whose optimum value is around 55%–65% [32]. Typically, the thermal engine has two or three operating points of different power level to be able to recharge the battery in different conditions, from very low to high power demands. In this study, to ensure that the series-hybrid vehicle reaches the rated torque and power of the conventional vehicle, three states for the thermal engine have been selected. The different engine states are represented in Fig. 7 over a NOx emissions map, and described in Table 6.

Together with the engine speed and torque, the other parameters selected to be optimized through the DoE + Kriging methodology are depicted in Table 7. To perform the optimization, a DoE with 800 points varying the battery capacity and the SOC difference (SOC_{dif}) is proposed. The parameter SOC_{dif} is used to modify the SOC interval limits (SOC_{ini}-SOC_{dif}), which define the transition between the different engine states according to the rule based control (RBC) strategy defined (Table 8). The initial SOC (SOC_{ini}) was fixed at 0.64 according to previous works [33]. Finally, it is interesting to remark that a mandatory constraint to select one result as valid is that the battery SOC level at the end of the cycle

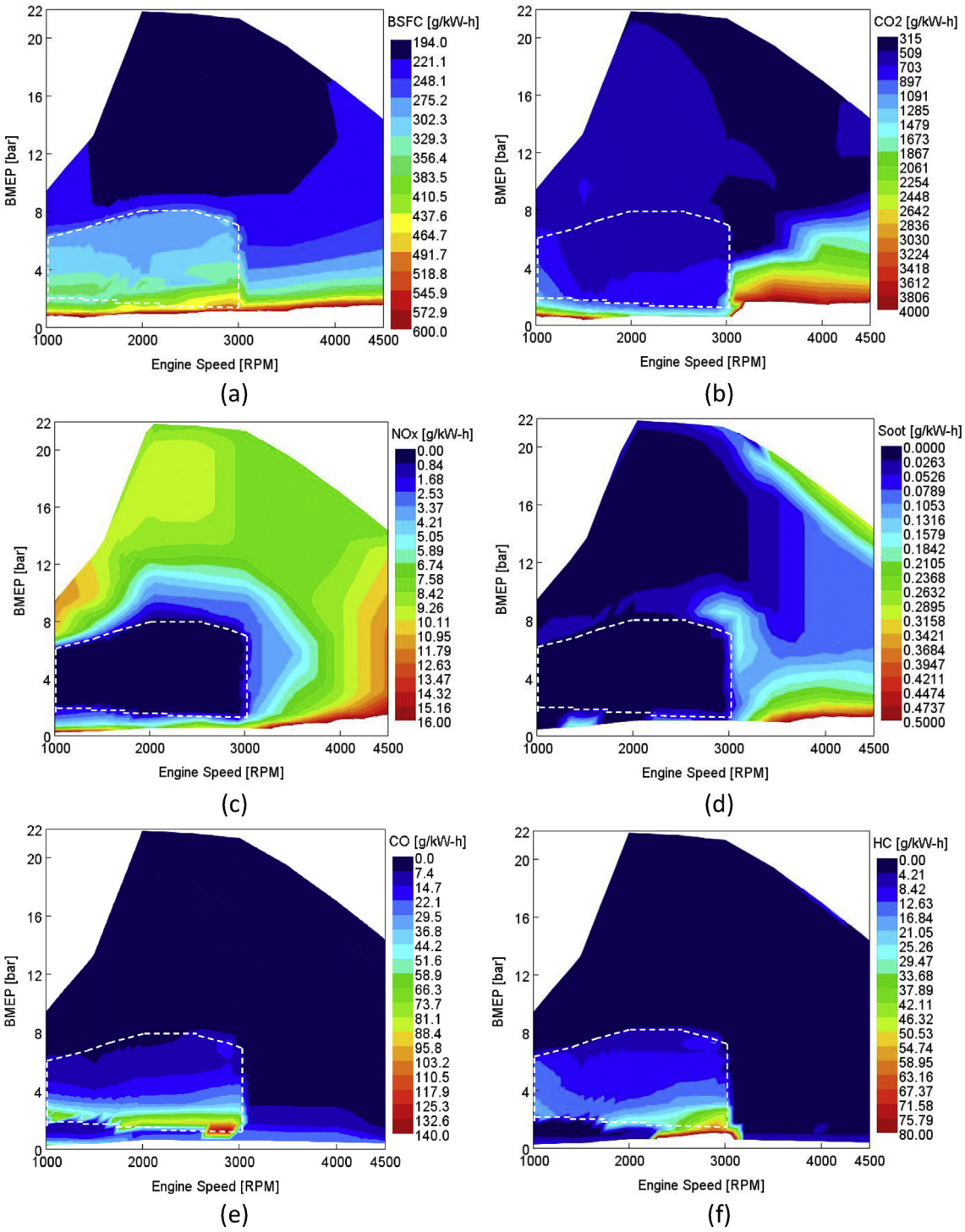

Fig. 5. Fuel consumption and engine-out emissions maps for the dual-duel E85-diesel concept.

must be equal or greater to that found at the beginning of the cycle ($SOC_{final} \geq SOC_{initial}$).

The rule-based control (RBC) used in this research relies on turning on, or switching the engine state according to pre-defined objectives. The control variable behavior informs the supervisory control about the real-time battery level, allowing to determine the next decision for the ICE. In this sense, the number of power levels as well as the operating conditions used to charge the batteries will have a direct impact on the performance during the driving cycle. The RBC strategy used in this work is summarized in Table 8. As it can be seen, the different conditional statements that will promote the transition of the ICE between the different states depend on the SOC_{dif}, which means that different RBC conditions will be tested during the optimization through the DoE.

From the 800 combinations proposed in the DoE, only 154 combinations were able to fulfill the restriction imposed about the battery SOC ($SOC_{final} \geq SOC_{initial}$). Fig. 8 shows the different points belonging to each these potential strategies. Moreover, the maximum torque and power lines of the conventional vehicle are represented. It is interesting to note that each of the 154 strategies has associated one point per each engine state. The use of each of the three operating points will depend on the

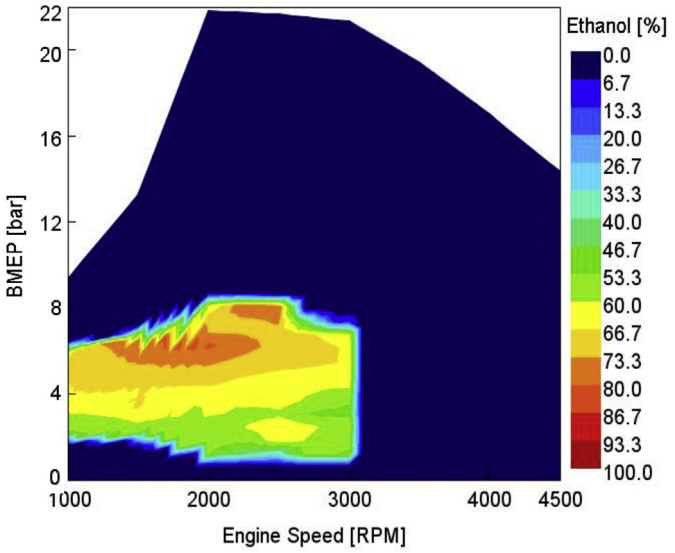

Fig. 6. Ethanol fraction map for the dual-duel E85-diesel concept.

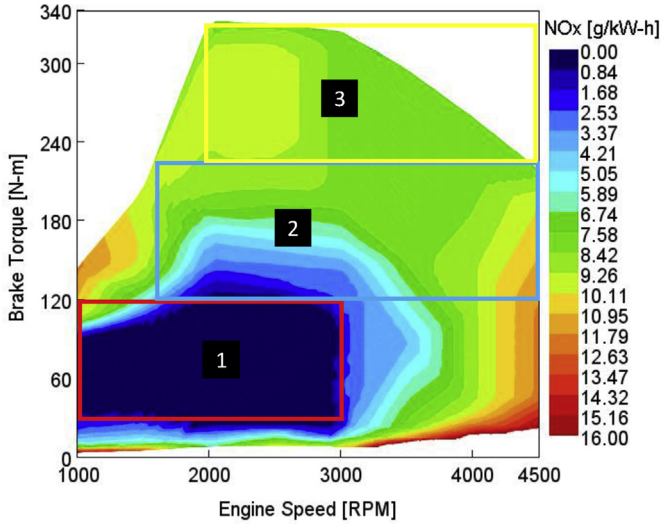

Fig. 7. Different engine states represented over a NOx emissions map.

Table 6
Description of the different states of the thermal engine.

Conditions	State 0	State 1	State 2	State 3
Engine on/off [−]	Off	On	On	On
Engine Speed [rpm]	–	1000–3000	1500–4500	2000–4500
Engine Torque [Nm]	–	30–120	120–230	230–330
Operation [−]	–	E85 dual-fuel	Diesel	Diesel

Table 7
Parameters varied in the DoE.

Parameter	Min	Max
Battery capacity [Ah]	10	80
SOC_{ini} [−]	0.64	
SOC_{dif} [−]	0.01	0.1

power level requested during the driving cycle.

After obtaining the DoE results, different response models were adjusted using the Kriging fitting method [30]. The goodness of the fit was assessed by the R^2 values and the graphical dispersion of the observed and predicted values for each dependent factor. As it can be seen in Fig. 9, a proper agreement is verified for the two response parameters, with the R^2 being 89% for the NOx emissions and 86% for the energy consumption. After that, new combinations were proposed to obtain the Pareto optimization by using the models adjusted with the Kriging method.

Table 8
RBC control strategy.

Conditional statement	Transitions
State = 0 & SOC < (SOC_{ini}-SOC_{dif})	CD State 0 to CS State 1
State = 1 & SOC < (SOC_{ini}- 2 * SOC_{dif})	CS State 1 to CS State 2
State = 2 & SOC < (SOC_{ini}- 3 * SOC_{dif})	CS State 2 to CS State 3
State = 3 & SOC > (SOC_{ini} - 2* SOC_{dif})	CS State 3 to CS State 2
State = 2 & SOC > (SOC_{ini}-SOC_{dif})	CS State 2 to CS State 1
State = 1 & SOC > SOC_{ini}	CS State 1 to CD State 0

Fig. 10 shows the trade-off between NOx and energy consumption for the 154 potential combinations that resulted from the DoE. All the points shown in the figure represent the result obtained with a control strategy that has the 3 engine states available to be used (Fig. 7). However, depending on the optimization, the different strategies can require using only one, two or three engine states to complete the driving cycle. The points shown in Fig. 10 are differentiated depending on the amount of engine states used to complete the WLTC cycle. Moreover, the Pareto frontier resulting from the Kriging fitting method is represented (359 points). As it can be seen, approximately 40% of the total strategies are able to obtain energy consumptions lower than the conventional diesel vehicle. However, only the strategy which works with the State 1 in the entire cycle is capable of reaching engine-out Euro 6 NOx limits. This result can be explained looking at Fig. 7, which shows that the State 1 matches with the dual-fuel E85 operation, which provides ultra-low engine-out emissions. The strategy working in the engine States 1 and 2 provides the lowest energy consumption. Looking at Fig. 6a, it can be seen that at medium load CDC operation has lower BSFC than dual-fuel E85, which explains the energy gain with the two-state strategy. On the other hand, it is seen that the three-state strategy has only two potential points, which are far from the limits imposed in terms of NOx emissions. This is because the third engine state implies using the thermal engine at high load under CDC conditions, which has a clear penalty on NOx emissions. Finally, the figure shows that one point of the one-state strategy falls into the predicted Pareto frontier through the Kriging method, so this point is selected as optimum case for the LTC-SHV configuration.

To extend the explanation done in Figs. 10 and 11 shows the energy consumption and NOx emissions as a function of the ethanol fraction consumed along the WLTC cycle. As it can be seen, using ethanol fractions of around 50%–70%, the NOx levels achieved are lower than CDC, while the only way to reach engine-out Euro 6 NOx levels is using ethanol fractions of around 75%–85%. The optimal case is marked a square in both subfigures.

The final parameters for the optimum case are summarized in Table 9. From the table, it can be seen that to allow using only the State 1 for the entire cycle, the SOC_{dif} was near the maximum proposed in the DoE. With this, a medium capacity battery (12 kWh) was enough to feed the system for the entire driving cycle. Finally, to be able to give the rated power and torque of the original engine, operating conditions for the State 2 and State 3 were also selected. These two conditions were selected to minimize the fuel consumption in their respective areas.

LTC-SHV performance and emissions

Fig. 12 shows the cumulated energy consumption and the battery SOC level along the WLTC cycle for the vehicle operating under CDC and optimized LTC-SHV conditions. Moreover, the evolution of the thermal engine state is depicted in the figure. Fig. 13 shows the same information for the RDE cycle. As it can be seen in both figures, in the case of the LTC-

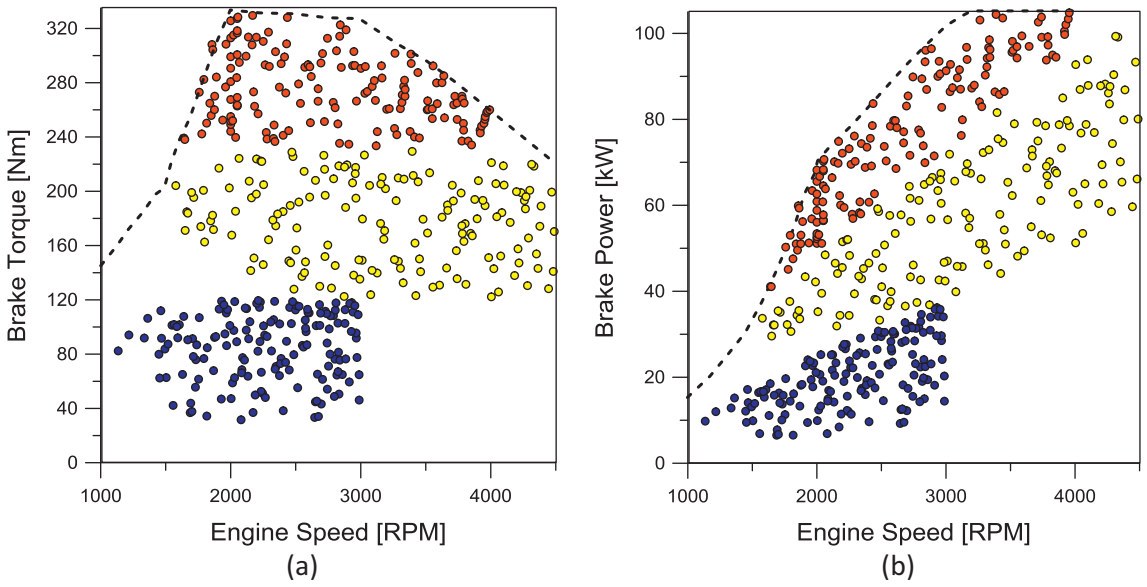

Fig. 8. Potential strategies (3 points each) represented on the Power (a) and Torque (b) engine map.

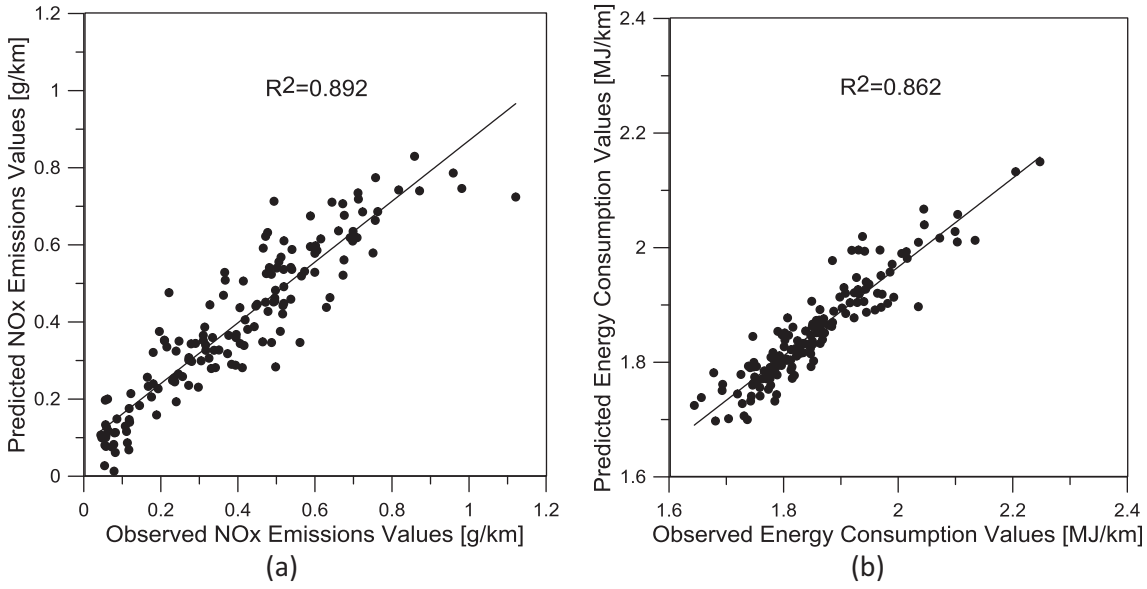

Fig. 9. Predicted vs observed values for the Pareto Frontier obtained with the Kriging fitting method.

SHV, the battery SOC level at the end of the cycle is equal to that found at the beginning of the cycle. In both driving cycles, the LTC-SHV concept allows reducing the final energy consumption as compared to CDC. In the case of the WLTC, the major part of the energy save comes from the low and medium phases, where it is not needed to start the thermal engine to reach the desired power levels. In this sense, with the initial battery SOC and the regenerative braking is enough to complete around 64% of the total cycle duration. After that, the energy slope for the LTC-SHV increases and it is maintained until reaching the end of the cycle because the ICE remains at the State 1. Comparing both vehicle concepts in the high phase of the WLTC, it is possible to see that the LTC-SHV has greater energy consumption than CDC due to the necessity of providing the power demanded and recharge the battery to the desired SOC. During the extra-high phase, the slope of the CDC vehicles equals of that of the LTC-SHV due to the higher power levels requested. In the case of the RDE, the large duration of the urban phase makes necessary to switch on the thermal engine during around 5 min, which penalizes the energy consumption during this phase. Comparing the SOC profile between both cycles in the low (WLTC) and urban (RDE) phases, it is seen that the SOC falls more rapidly for the RDE case, which is consequence of the greater number of accelerations in the driving pattern. As in the case of the WLTC, the thermal engine needs to be used during the majority of the rural phase, and during the total duration of the highway phase.

Tables 10 and 11 show the fuel and energy consumption as well as the engine-out emissions for CDC and LTC-SHV conditions at the end of the WLTC and RDE cycle, respectively. In both cases, the total fuel consumption for the LTC-SHV is greater than the conventional powertrain, which is consequence of the low LHV of E85 (Table 3). By contrast, when comparing the energy consumption, it is seen that LTC-SHV allows a reduction from 3% to 6.5% compared to CDC in the final energy consumed. To reach this value, 82% of the total fuel consumed during LTC-SHV operation is E85. In terms of engine-out emissions, it is seen that the conventional vehicle surpasses by far all the limits imposed by the Euro 6 regulation for all the pollutants. So, a conventional aftertreatment layout with DOC, diesel oxidation catalyst (DPF) and selective catalytic reduction (SCR) will be needed to reach the regulation levels at

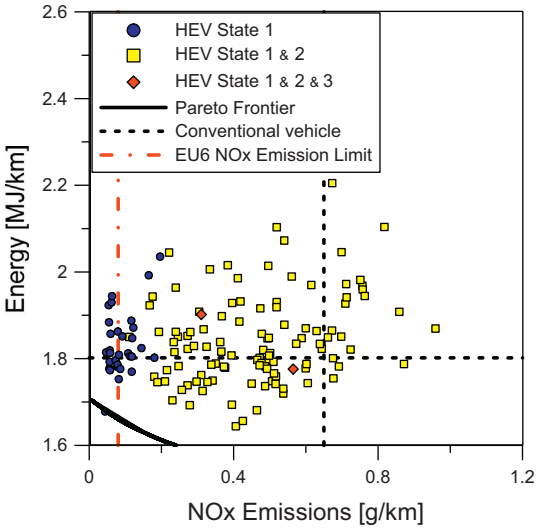

Fig. 10. Trade-off between the energy consumption and NOx emission for the hybrid series vehicle along the WLTC driving cycle.

the tail-pipe. By contrast, it can be seen that the LTC-SHV concept is able to reach Euro 6 engine-out NOx and soot levels. Moreover CO_2 is reduced by 16% compared to CDC. As a counterpart, HC + NOx and CO emissions exceed by far the normative values. To meet the regulation levels for these pollutants, it will be needed to add a DOC system to the vehicle.

Previous investigations have evaluated experimentally the efficiency of a conventional DOC when used for dual-fuel combustion [27]. The experimental results obtained were promising, reaching 100% and 95% conversion efficiency levels for CO and HC, respectively, after reaching the light-off temperature (~200 °C). With these results, a DOC model for dual-fuel vehicles was built in previous works [33]. Fig. 14 shows the engine-out and tail-pipe HC and CO levels when using a DOC sized for the ICE used in this study. In this case, the estimated CO and HC conversion efficiency levels for the dual-fuel

Table 9
Parameters for the optimal case.

Parameter	Value
Battery capacity [Ah]	32
SOC_{dif} [−]	0.09
State 1 [rpm/Nm]	2280/93
State 2 [rpm/Nm]	2600/175
State 3 [rpm/Nm]	3000/280
Vehicle added weight [kg]	170
Vehicle total weight [kg][a]	1693

[a] Without passenger and cargo.

combustion were 97% and 98% respectively, while for the pure diesel case were 95% and 96%.

Conclusions

This work investigated the potential of a series hybrid vehicle concept that combines low temperature combustion and biofuels as power source. To do this, experimental data from a SCE running under ethanol-diesel dual-fuel combustion was used. Then, vehicle systems simulations were used to estimate performance and emissions of the hybrid vehicle and compare them versus conventional diesel combustion. The vehicle selected to perform the simulations is the Opel Vectra, which equips the compression ignition engine used in the experimental tests.

Before reaching the final results from the simulations, a multi-objective optimization was done to determine some characteristics and controls of the hybrid vehicle. To do this, a methodology combining DoE and the Kriging fitting method was used taking the WLTC cycle as reference. With this, the optimum battery capacity was found to be 32 Ah. Moreover, it was concluded that the optimal control strategy only needs the ICE working at the State 1 (low power) to fulfill the requirements imposed by both the WLTC and RDE cycle.

The comparison of the estimated performance and emissions of the LTC-hybrid concept versus CDC over the WLTC and RDE cycles revealed clear benefits in terms of energy consumption, CO_2 and NOx and soot emissions. In this sense, the hybrid concept enabled a reduction of the final energy consumed of 3% in RDE cycle and 6.5% in the WLTC

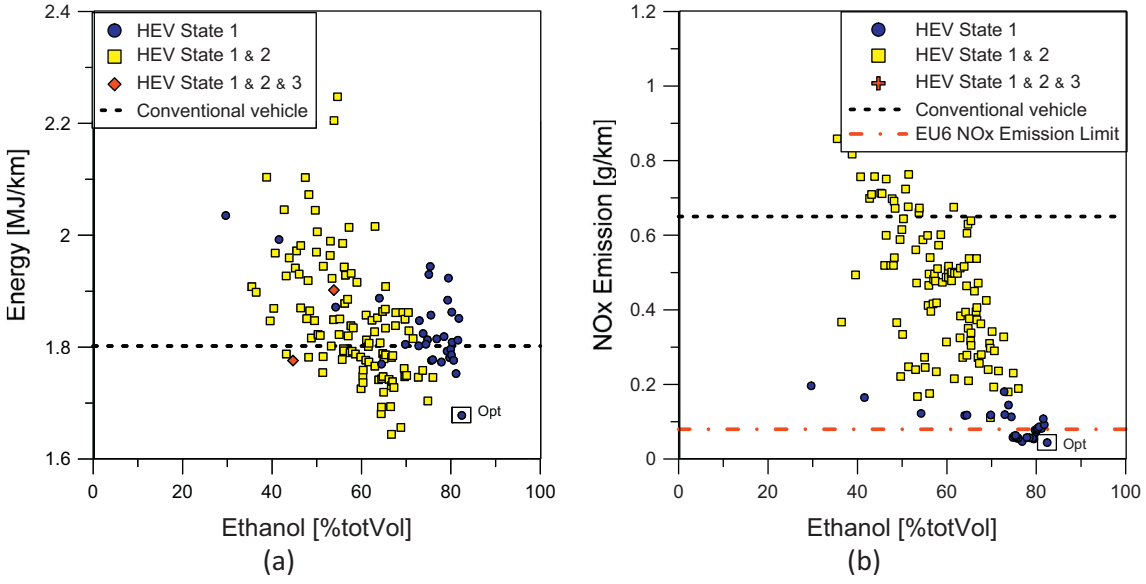

Fig. 11. Energy Consumption (a) and NOx emissions (b) as a function of ethanol fraction used for the LTC-SHV along the WLTC cycle in the different configurations studied in the DoE.

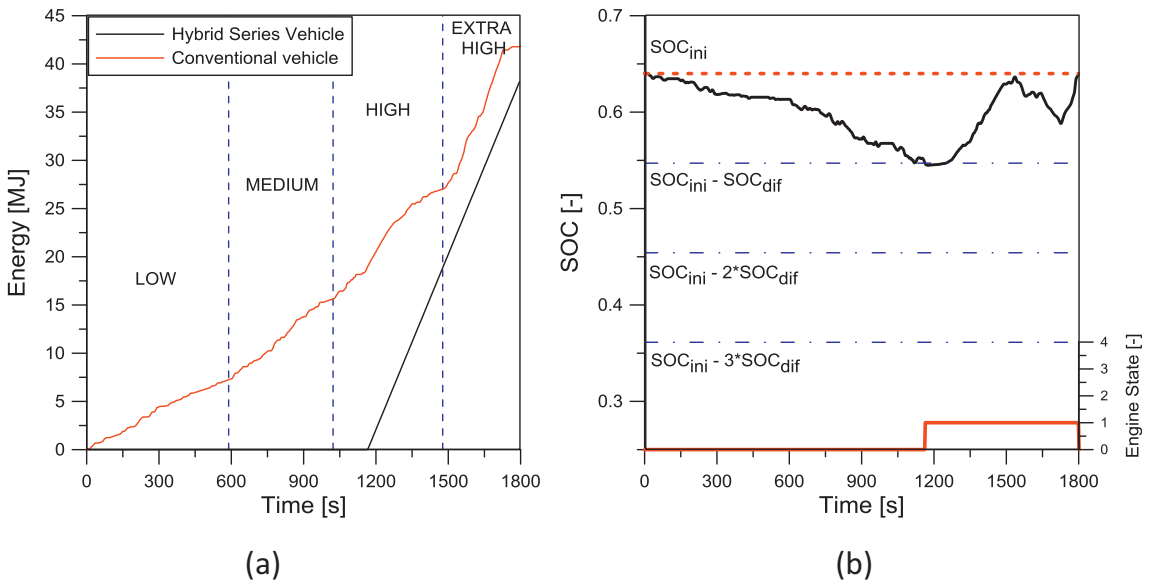

Fig. 12. Energy Consumption for conventional and series hybrid vehicle along the WLTC driving cycle (a). Battery SOC level and engine state along WLTC driving cycle for the optimum LTC-SHV case (b).

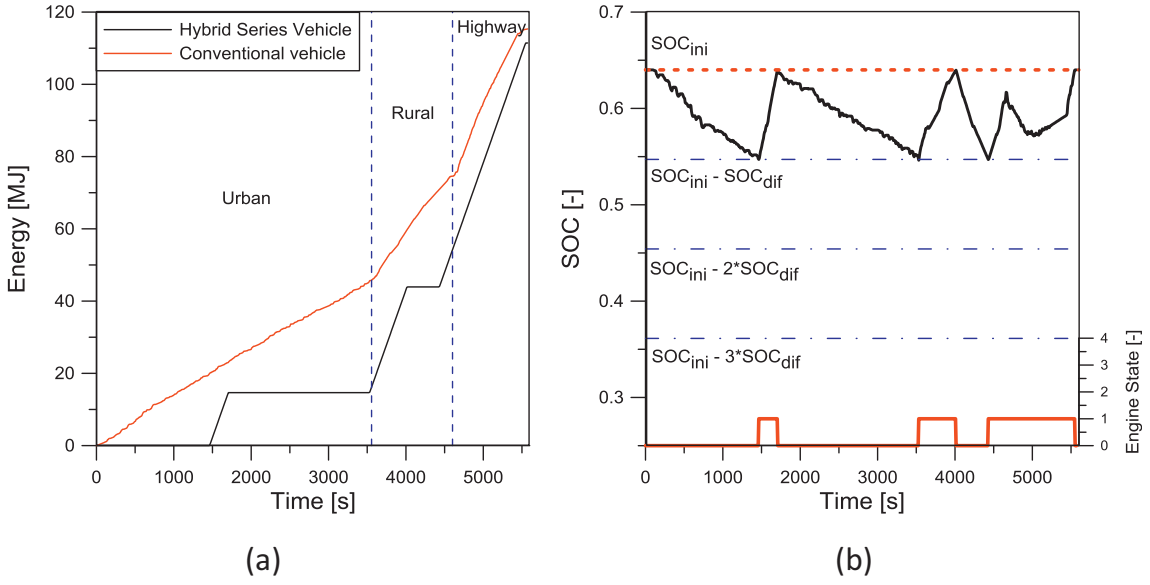

Fig. 13. Energy Consumption for conventional and series hybrid vehicle along the RDE driving cycle (a). Battery SOC level and engine state along RDE driving cycle for the optimum LTC-SHV case (b).

Table 10
Fuel consumption and engine-out emissions for the two vehicles at WLTC driving cycle.

Parameter	Conventional Vehicle	Series Hybrid Vehicle	EU 6 limits for WLTC
Fuel [L/100 km]	5.0	6.3	–
Energy [MJ/km]	1.80	1.68	–
Ethanol/Tot Fuel [% vol]	–	82	–
NO_x [g/km]	0.65	0.04	0.08
HC + NO_x [g/km]	0.77	1.79	0.17
CO [g/km]	0.68	1.97	0.5
Soot [g/km]	0.0086	0.0001	0.005
CO_2 [g/km]	127	106	–

Table 11
Fuel consumption and engine-out emissions for the two vehicles at RDE driving cycle.

Parameter	Conventional Vehicle	Hybrid Series Vehicle	EU 6 limits for WLTC
Fuel [L/100 km]	4.79	6.22	–
Energy [MJ/km]	1.71	1.66	–
Ethanol/Tot Fuel [% vol]	–	82	–
NO_x [g/km]	0.49	0.04	0.08
HC + NO_x [g/km]	0.62	1.76	0.17
CO [g/km]	0.69	1.94	0.5
Soot [g/km]	0.0089	0.0001	0.0050
CO_2 [g/km]	120	105	–

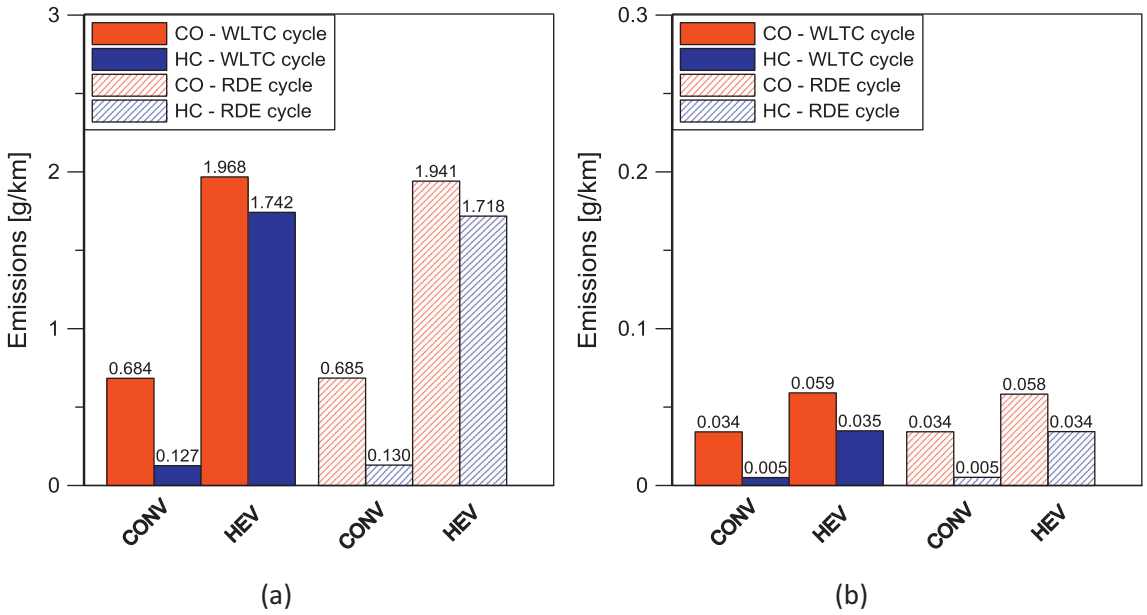

Fig. 14. Engine-out (a) and estimated tail-pipe HC and CO levels (b) for the LTC-SHV concept. Results are estimated using a DOC model calibrated for dual-fuel combustion.

compared to CDC. In terms of engine-out emissions, CO_2 were reduced around 16% versus CDC, and engine-out NOx and soot were reduced below the levels imposed by the Euro 6 regulation. As a penalty, the engine-out HC and CO emissions increased to more than double than CDC. However, based on previous experimental results, it is expected that a conventional DOC can reduce the tail-pipe HC and CO levels below the Euro 6 limits.

Acknowledgments

The authors gratefully acknowledge General Motors Global Research & Development for providing the engine used to acquire the experimental data shown in this investigation. The authors also acknowledge FEDER and Spanish Ministerio de Economía y Competitividad for partially supporting this research through TRANCO project (TRA2017-87694-R).

References

[1] The automobile industry pocket guide 2015-2016, European Automobile Manufacturers' Association's (ACEA), Brussels, 2016.
[2] G. Kalghatgi, Is it really the end of internal combustion engines and petroleum in transport? Appl. Energy Appl. Energy 225 (May 2018) 965–974.
[3] S. Singh, C. Kennedy, Estimating future energy use and CO2 emissions of the world's cities, Environ. Pollut. 203 (August 2015) 271–278.
[4] M. Engel, B. Paas, C. Schneider, C. Pfaffenbach, J. Fels, Perceptual studies on air quality and sound through urban walks, Cities 83 (31 December 2018) 173–185.
[5] J. Guanetti, S. Formentin, M. Corno, S. Savaresi, Optimal energy management in series hybrid electric bicycles, Automatica 81 (July 2017) 96–106.
[6] H. He, X. Guo, Multi-objective optimization research on the start condition for a parallel hybrid electric vehicle, Appl. Energy 227 (1 October 2018) 294–303.
[7] Y. Tian, W. Sun, D. Qu, L. Wang, Study of a exhaust after-treatment system Applied to hybrid vehicle, in: 2011 asia-pacific power and energy engineering conference, 2011, pp. 1–4, https://doi.org/10.1109/APPEEC.2011.5748870. Wuhan.
[8] F. Posada, S. Chambliss, K. Blumberg, Costs of emission reduction technologies for heavy-duty diesel vehicles, ICCT White Paper (2016).
[9] P. García-Valladolid, P. Tunestal, J. Monsalve-Serrano, A. García, J. Hyvönen, Impact of diesel pilot distribution on the ignition process of a dual fuel medium speed marine engine, Energy Convers. Manag. 149 (1 Oct 2017) 192–205.
[10] H.W. Wu, R.H. Wang, D.J. Ou, Y.C. Chen, T.Y. Chen, Reduction of smoke and nitrogen oxides of a partial HCCI engine using premixed gasoline and ethanol with air, Appl. Energy 88 (11) (November 2011) 3882–3890, 2011-90-80.
[11] P. Olmeda, A. García, J. Monsalve-Serrano, R. Sari, Experimental investigation on RCCI heat transfer in a light-duty diesel engine with different fuels, Comparison versus conventional diesel combustion, Appl. Therm. Eng. 144 (November 2018) 424–436.
[12] M. Yao, Z. Zheng, H. Liu, Progress and recent trends in homogeneous charge compression ignition (HCCI) engines, Prog. Energy Combust. Sci. 35 (Issue 5) (2009) 398–437.
[13] R. Maurya, A. Agarwal, Experimental investigation on the effect of intake air temperature and air–fuel ratio on cycle-to-cycle variations of HCCI combustion and performance parameters, Appl. Energy 88 (2011) 1153–1163.
[14] A. Singh, A. Agarwal, Combustion characteristics of diesel HCCI engine, an experimental investigation using external mixture formation technique, Appl. Energy 99 (2012) 116–125.
[15] Y. Yang, J. Dec, N. Dronniou, M. Sjöberg, Tailoring HCCI heat-release rates with partial fuel stratification, Comparison of two-stage and single-stage-ignition fuels, Proc. Combust. Inst. 33 (2) (2011) 3047–3055.
[16] G.T. Kalghatgi, Auto-ignition quality of practical fuels and implications for fuel requirements of future SI and HCCI engines, 2005. SAE paper 2005-01-0239.
[17] K. Inagaki, T. Fuyuto, K. Nishikawa, K. Nakakita, I. Sakata, Dual-fuel PCI combustion controlled by in-cylinder stratification of ignitability, 2006. SAE Technical Paper 2006-01-0028.
[18] J. Benajes, A. García, J. Monsalve-Serrano, I. Balloul, G. Pradel, Evaluating the reactivity controlled compression ignition operating range limits in a high-compression ratio medium-duty diesel engine fueled with biodiesel and ethanol, Int. J. Engine Res. 18 (1–2) (2017) 66–80.
[19] A. García, J. Monsalve-Serrano, V. Rückert Roso, M. Santos Martins, Evaluating the emissions and performance of two dual-mode RCCI combustion strategies under the World Harmonized Vehicle Cycle (WHVC), Energy Convers. Manag. 149 (2017) 263–274.
[20] J. Benajes, A. García, J. Monsalve-Serrano, D. Villalta, Exploring the limits of the reactivity controlled compression ignition combustion concept in a light-duty diesel engine and the influence of the direct-injected fuel properties, Energy Convers. Manag. 157 (February 2018) 277–287.
[21] J. Benajes, A. García, J. Monsalve-Serrano, I. Balloul, G. Pradel, An assessment of the dual-mode reactivity controlled compression ignition/conventional diesel combustion capabilities in a EURO VI medium-duty diesel engine fueled with an intermediate ethanol-gasoline blend and biodiesel, Energy Convers. Manag. 123 (July 2016) 381–391.
[22] J. Benajes, A. García, J. Monsalve-Serrano, V. Boronat, Dual-fuel combustion for future clean and efficient compression ignition engines, Appl. Sci. 7 (1) (2017) 36.
[23] J. Benajes, A. García, J. Monsalve-Serrano, V. Boronat, An investigation on the particulate number and size distributions over the whole engine map from an optimized combustion strategy combining RCCI and dual-fuel diesel-gasoline, Energy Convers. Manag. 140 (15 May 2017) 98–108.
[24] J. Benajes, A. García, J. Monsalve-Serrano, V. Boronat, Gaseous emissions and particle size distribution of dual-mode dual-fuel diesel-gasoline concept from low to full load, Appl. Therm. Eng. 120 (2017) 138–149.
[25] Curran S, Hanson R, Wagner R. Reactivity controlled compression ignition combustion on a multi-cylinder light-duty diesel engine. Int. J. Engine Res. 13 (3), 216-225.
[26] R.D. Reitz, G. Duraisamy, Review of high efficiency and clean reactivity controlled compression ignition (RCCI) combustion in internal combustion engines, Prog. Energy Combust. Sci. 46 (February 2015) 12–71.
[27] J. Benajes, A. García, J. Monsalve-Serrano, R. Sari, Experimental investigation on the efficiency of a diesel oxidation catalyst in a medium-duty multi-cylinder RCCI engine, vol. 176, 15 November 2018, pp. 1–10.

[28] P. Olmeda, J. Martin, A. Garcia, D. Villalta, A. Warey, V. Domenech, A combination of swirl ratio and injection strategy to increase engine efficiency, SAE Int. J. Engine. 10 (3) (2017), https://doi.org/10.4271/2017-01-0722.
[29] J.M. Luján, V. Bermúdez, V. Dolz, J. Monsalve-Serrano, An assessment of the real-world driving gaseous emissions from a Euro 6 light-duty diesel vehicle using a portable emissions measurement system (PEMS), Atmos. Environ. 174 (Feb 2018) 112–121.
[30] M. Oliver, R. Webster, Kriging, a method of interpolation for geographical information systems, Int. J. Geogr. Inf. Syst. 4 (3) (1990) 313–332.
[31] J. Benajes, A. García, J. Monsalve-Serrano, D. Villalta, Benefits of E85 versus gasoline as low reactivity fuel for an automotive diesel engine operating in reactivity controlled compression ignition combustion mode, Energy Convers. Manag. 159 (2018) 85–95.
[32] J. Benajes, A. García, J. Monsalve-Serrano, R. Sari, Potential of RCCI series hybrid vehicle architecture to meet the future CO2 targets with low engine-out emissions, Appl. Sci. 6 (August 2018).
[33] A. García, P. Piqueras, J. Monsalve-Serrano, R. Sari, Sizing a conventional diesel oxidation catalyst to be used for RCCI combustion under real driving conditions, Appl. Therm. Eng. 140 (July 2018) 62–72.